

# Overview of New Tools to Perform Safety Analysis: BWR Station Black Out Test Case

D. Mandelli<sup>a\*</sup>, C. Smith<sup>a</sup>, T. Riley<sup>c</sup>, J. Nielsen<sup>a</sup>, J. Schroeder<sup>a</sup>, C. Rabiti<sup>a</sup>, A. Alfonsi<sup>a</sup>, J. Cogliati<sup>a</sup>,  
R. Kinoshita<sup>a</sup>, V. Pascucci<sup>b</sup>, B. Wang<sup>b</sup>, D. Maljovec<sup>b</sup>

<sup>a</sup>Idaho National Laboratory, Idaho Falls (ID), USA

<sup>b</sup>University of Utah, Salt Lake City (UT), USA

<sup>c</sup>Oregon State University, Corvallis (OR), USA

---

**Abstract:** The existing fleet of nuclear power plants is in the process of extending its lifetime and increasing the power generated from these plants via power uprates. In order to evaluate the impacts of these two factors on the safety of the plant, the Risk Informed Safety Margin Characterization project aims to provide insights to decision makers through a series of simulations of the plant dynamics for different initial conditions (e.g., probabilistic analysis and uncertainty quantification). This paper focuses on the impacts of power uprate on the safety margin of a boiling water reactor for a station black-out event. Analysis is performed by using a combination of thermal-hydraulic codes and a stochastic analysis tool currently under development at the Idaho National Laboratory, i.e. RAVEN. We employed both classical statistical tools, i.e. Monte-Carlo, and more advanced machine learning based algorithms to perform uncertainty quantification in order to quantify changes in system performance and limitations as a consequence of power uprate. We also employed advanced data analysis and visualization tools that helped us to correlate simulation outcomes such as maximum core temperature with a set of input uncertain parameters. Results obtained give a detailed investigation of the issues associated with a plant power uprate including the effects of station black-out accident scenarios. We were able to quantify how the timing of specific events was impacted by a higher nominal reactor core power. Such safety insights can provide useful information to the decision makers to perform risk-informed margins management.

**Keyword:** Dynamic PRA, SBO, BWR, data analysis, adaptive sampling, topological analysis

---

## 1. INTRODUCTION

In the RISMC [1] approach, what we want to understand is not just the frequency of an event like core damage, but how close we are (or not) to key safety-related events and how might we increase our safety margin through proper application of Risk Informed Margin Management. In general terms, a “margin” is usually characterized in one of two ways:

- A deterministic margin, typically defined by the ratio (or, alternatively, the difference) of a capacity (i.e., strength) over the load.
- A probabilistic margin, defined by the probability that the load exceeds the capacity.

A probabilistic safety margin is a numerical value quantifying the probability that a safety metric (e.g., for an important process observable such as clad temperature) is exceeded under accident conditions.

The RISMC Pathway uses the probabilistic margin approach to quantify impacts to reliability and safety. As part of the quantification, we use both probabilistic (via risk simulation) and mechanistic (via physics models) approaches. Probabilistic analysis is represented by the stochastic risk analysis while mechanistic analysis is represented by the plant physics calculations. Safety margin and uncertainty quantification rely on plant physics (e.g., thermal-hydraulics and reactor kinetics) coupled with probabilistic risk simulation. The coupling, which we call Computational PRA (CPRA), takes place through the interchange of physical parameters (e.g., pressures and temperatures) and operational or accident scenarios (e.g., the series of successes and/or failures representing a sequence of events).

This paper presents a case study in order to show the capabilities of the RISMC methodology [4] to assess limitations and performances of a Boiling Water Reactor (BWR) system during a Station Black

---

\* Corresponding author: Diego Mandelli, P.O. Box 1625, MS 3850, Idaho Falls 83415 (ID); diego.mandelli@inl.gov

Out (SBO) accident scenario using a simulation-based environment also known as dynamic PRA [2]. Such assessment cannot be naturally performed in a classical ET/FT based environment. We employ a system simulator code, one of the RELAP series of codes [3], coupled with a CPRA [2] code, RAVEN [5,6], that monitors and controls the simulation. The latter code, in particular, introduces both deterministic (e.g., system control logic, operating procedures) and stochastic (e.g., component failures, variable uncertainties, human actions) elements into the simulation.

This paper is structured as follows:

- Sections 2 and 3 describe the BWR system and the SBO scenario
- Section 4 presents the evaluation of the safety margins
- Section 5 describes adaptive sampling algorithms in order to reduce computational time
- Section 6 shows the stochastic analysis performed with RAVEN coupled with RELAP-5
- Section 7 presents the analysis of the data generated in Section 6.

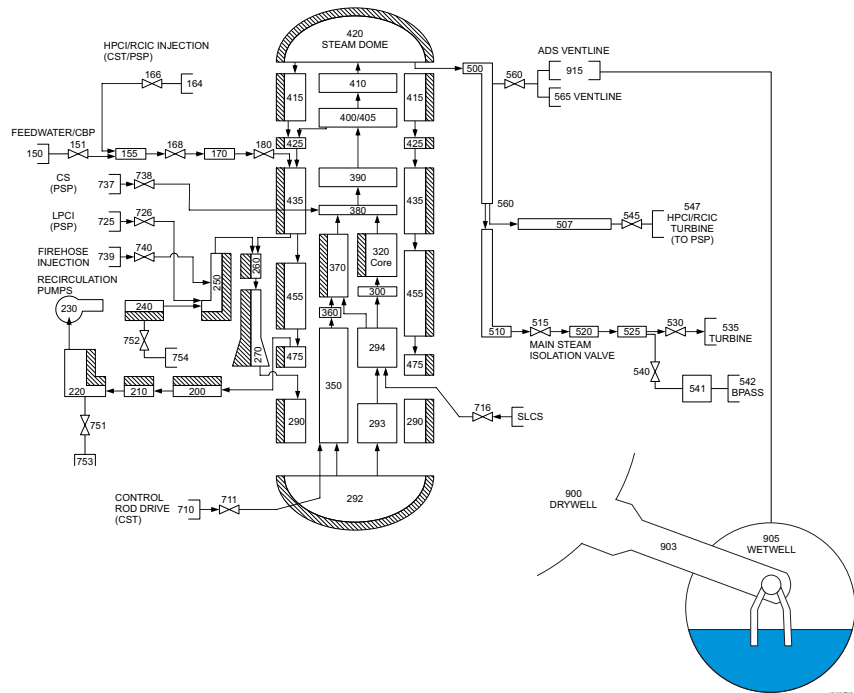


Figure 1: RELAP-5 nodalization scheme for the BWR system

## 2. BWR SYSTEM

The system considered in this test case is a generic BWR power plant with a Mark I containment as shown in Figure 1. The three main structures are the following:

- 1) Reactor Pressure Vessel (RPV), it is the pressurized vessel that contains the reactor core.
- 2) Primary containment includes:
  - a) Drywell (DW): it contains the RPV and circulation pumps
  - b) Pressure Suppression Pool (PSP) also known as wetwell: a large torus shaped container that contains a large amount of water; it is used as ultimate heat sink.
  - c) Reactor circulation pumps

While the original BWR Mark I includes a large number of systems, we consider a subset of it:

- RPV level control systems: provide manual/automatic control of the RPV water level:
  1. Reactor Core Isolation Cooling System (RCIC): Provide high-pressure injection of water from the CST to the RPV. Water flow is provided by a turbine driven pump that takes steam from the main steam line and discharges it to the suppression pool. Alternatively, the water source can be shifted from the CST to the PSP.
  2. High Pressure Coolant Injection (HPCI): similar to RCIC, it allows greater water flow rates
- Safety Relief Valves (SRVs): DC powered valves that control and limit the RPV pressure.

- Automatic Depressurization System (ADS): separate set of relief valves that are employed in order to depressurize the RPV.
- Cooling water inventory:
  1. Condensate Storage Tank (CST) that contains fresh water that can be used to cool the reactor core.
  2. PSP water: PSP contains a large amount of fresh water that is used to provide ultimate heat sink when AC power is lost.
  3. Firewater system: water contained in the firewater system can be injected into the RPV when other water injection systems are disabled and when RPV is depressurized.
- Power systems:
  1. Two independent power grids that are connected to the plant station through two independent switchyards. Loss of power from both switchyards disables the operability of all system except: ADS, SRV, RCIC and HPCI (which require only DC battery).
  2. Diesel generators (DGs) which provide emergency AC power
  3. Battery systems: instrumentation and control systems need DC power.

## 2.1 BWR Containment Management

In an accident scenario, the set of emergency operating procedures requires the reactors operators to monitor not just the RPV but also the containment (both DW and PSP) thermo-hydraulic parameters (level, pressure and temperature). In particular, a set of limit curves is provided so that when they are crossed, the operators are required to activate the ADS system. These limit curves, also known as Heat Capacity Temperature Limits (HCTL), are shown in Figure 2 for both PSP and DW.

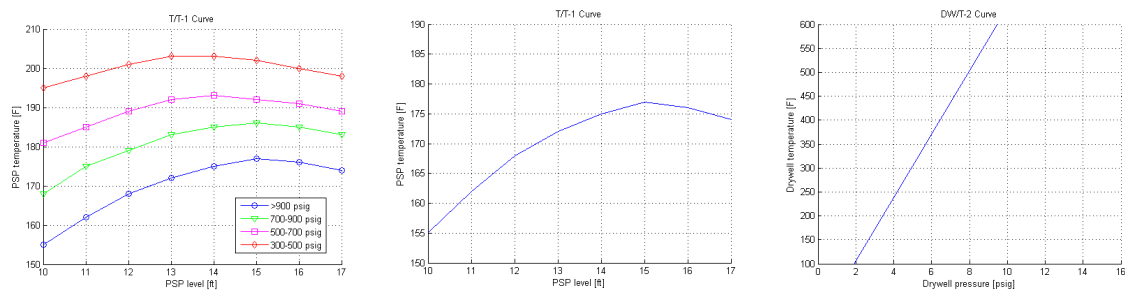


Figure 2: HTCLs for PSP (left and centre) and DW (right)

## 3. BWR SBO SCENARIO

The accident scenario under consideration is a loss of off-site power followed by loss of the DGs, i.e. SBO initiating event. In more details:

- At time  $t = 0$ : the following events occur:
  - LOOP condition occurs due to external events (i.e., power grid related)
  - LOOP alarm triggers the following actions:
    - Operators successfully scram the reactor and put it in sub-critical conditions by fully inserting the control rods in the core
    - Emergency DGs successfully start, i.e., AC power is available
    - Core decay heat is removed from the RPV through the RHR system
    - DC systems (i.e., batteries) are functional
- SBO condition occurs: due to internal failure, the set of DGs fails, thus removal of decay heat is impeded. Reactor operators start the SBO emergency operating procedures and perform:
  - RPV level control using RCIC or HPCI
  - RPV pressure control using SRVs
  - Containment monitoring (both drywell and PSP)
- Plant operators start recovery operations to bring back on-line the DGs while the recovery of the power grid is underway by the grid owner emergency staff
- Due to the limited life of the battery system and depending on the use of DC power, battery power can deplete. When this happens, all remaining control systems are offline causing the reactor core to heat until clad failure temperature is reached, i.e., core damage (CD)

- If DC power is still available and one of these conditions are reached:
  - Failure of both RCIC and HPCI
  - HCTL limits reached
  - Low RPV water level
 then the reactor operators activate the ADS system in order to depressurize the RPV
- Firewater injection: as an emergency action, when RPV pressure is below 100 psi plant staff can connect the firewater system to the RPV in order to cool the core and maintain an adequate water level. Such task is, however, hard to complete since physical connection between the firewater system and the RPV inlet has to be made manually.
- When AC power is recovered, through successful re-start/repair of DGs or off-site power, RHR can be now employed to keep the reactor core cool

### 3. STOCHASTIC MODELING

The choice of the set of stochastic parameters to consider in the analysis was based on the preliminary PRA model results obtained for a typical BWR SBO case. For all basic events (e.g., DG fail to run) we have considered the following indexes:

- Fussell-Vesely and Birnbaum importance
- Event-tree structure for a LOOP-SBO

The most relevant basic events obtained from the PRA model are listed in Table 1. Ultimately, we also included uncertainties associated with two additional parameters:

- Clad damage temperature
- Reactor initial power (ranging from 100% to 120%)

**Table 1: Basic Events obtained from the PRA model**

1	Failure time of DGs	5	RCIC fails to run time
2	Offsite AC power recovery time	6	SRVs stuck open time
3	Recovery time of DGs	7	Battery life
4	HPCI fails to run time		

#### 3.1 Human interventions

The probabilistic modeling of the five human interventions was done by looking at the SPAR-H [13] model from a generic BWR PRA. In this respect, we have identified 3 actions:

1. Manual ADS activation: operator manually depressurizes the RPV by activation the ADS system after HCTL limits are reached
2. Extended ECCS operation: operators may extend RCIC/HPCI and SRVs control even after the batteries have been depleted. This action actually summarizes two events:
  - a. Manually control RCIC/HPCI by acting on the steam inlet valve of the turbine
  - b. Alternate DC power availability through spare batteries
3. Firewater injection availability time (measured after ADS has been activated)

In general, SPAR-H characterizes each operator action through eight parameters – for this study we focused on just three factors: stress level, task complexity and time available to perform such task.

These three parameters are used in the SPAR model to compute the probability that such action will happen or not. However, from a simulation point of view we are not seeking *if* an action is performed but rather *when* such action is performed. Thus, we used the three factors mentioned above to determine the characteristic parameters (i.e., mean and standard deviation) of probability distribution function (assumed to be lognormal) that such action will occur as function of time.

### 4. SAFETY MARGIN ANALYSIS

This section shows some of the preliminary results regarding the effect of power uprates on SBO accident scenario. A higher value of thermal power generated in the core causes the following:

1. Faster heating of the PSP and, thus, a reduction of the time interval between ADS activation time and loss of DG time, i.e.,  $T_{ADS} - T_{SBO}$

2. A faster core temperature increase rate after ADS activation; thus leading to less time available to the plant staff to align the firewater

In summary, we expect that a power uprate reduces the time available to the plant staff to recover AC power and the time available to the plant staff to align FW (see Figure 3)

Scope of this section is to measure such reductions.

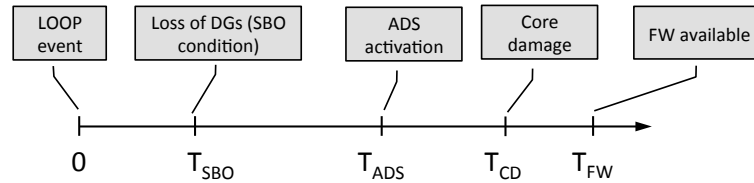


Figure 3: Typical SBO sequence of events

We performed an initial evaluation of the impact of power uprate by observing the PSP temperature increase rate as function of the thermal power generated by the core (see left image of Figure 4). In particular, we looked at the time to reach the PSP temperature limits for different values of core power (ranging from 100% to 120%). These results are shown on the right image of Figure 4. For this set of simulations we fixed  $T_{SBO} = 1\text{h}$  and we, thus, measured  $T_{ADS} - T_{SBO}$ .

As expected, by increasing the core power, the time to reach the PSP heat capacity limits decrease. In the left graph in Figure 4, the PSP temperature can be seen increasing in small steps as the SRVs open and close, and remaining relatively flat for a longer period of time whenever HPCI/RCIC activates and it is unnecessary to open the SRVs for a longer period of time. The sudden large increase in PSP temperature in each simulation is when the PSP heat capacity limit is reached and the ADS activates, dumping a huge amount of steam from the RPV into the PSP. Note that (Figure 4 right), if reactor power is increased to 110% and 120%, the time to reach core HCTL limits decrease from 4.5 h (16300 s) to 3.9 h (14100 s) and 3.5 h (12400 s) respectively.

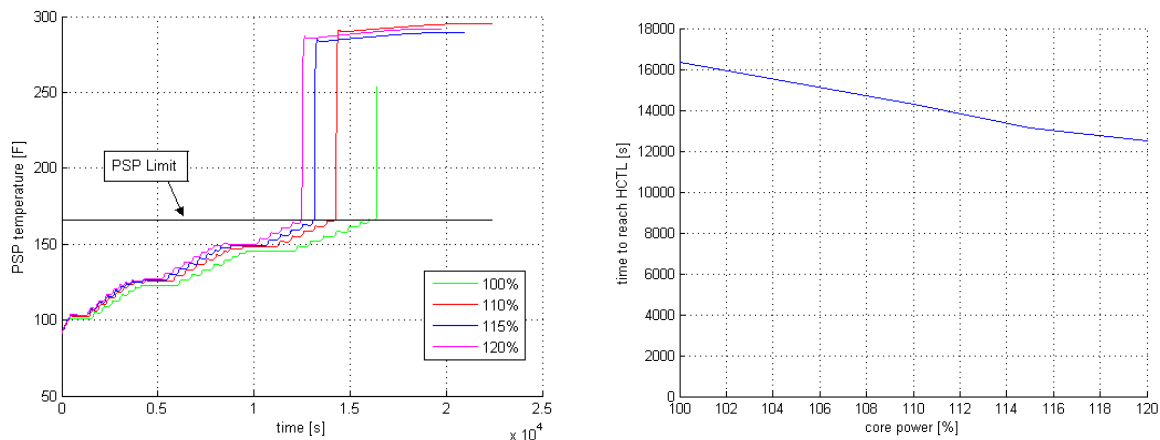


Figure 4: Impact of reactor power uprate on time to reach PSP heat capacity limits HCTL

We then considered the impact of power uprate for the following cases:

- Time to activate ADS vs. DG failure time (see Figure 5 left)
- Time to reach core damage vs. DG failure time (see Figure 5 right)

From Figure 5 note the following:

- We selected, for each power level (100%, 110% and 120%), a set of values for  $T_{SBO}$ . We then run a set of simulation runs and identified that time at which the reactor operators needs to activate the ADS. Compared to what is presented in Figure 4, this analysis considered not just PSP temperature as indication to trigger ADS activation but all the curves shown in Figure 2. In addition, AC power is not recovered and FW is never available.
- Figure 5 (left) shows  $T_{SBO}$  (x axis) vs.  $T_{ADS} - T_{SBO}$  (y axis). By increasing  $T_{SBO}$ , we expect that the reactor operators are required to activate ADS much later. Again, a reactor power increase negatively affects ADS activation time.
- Figure 5 (right) shows  $T_{SBO}$  (x axis) vs.  $T_{CD} - T_{SBO}$  (y axis). If AC power is available for a long time, the PSP HCTL limits are reached further in time. This allows reaching CD much later.

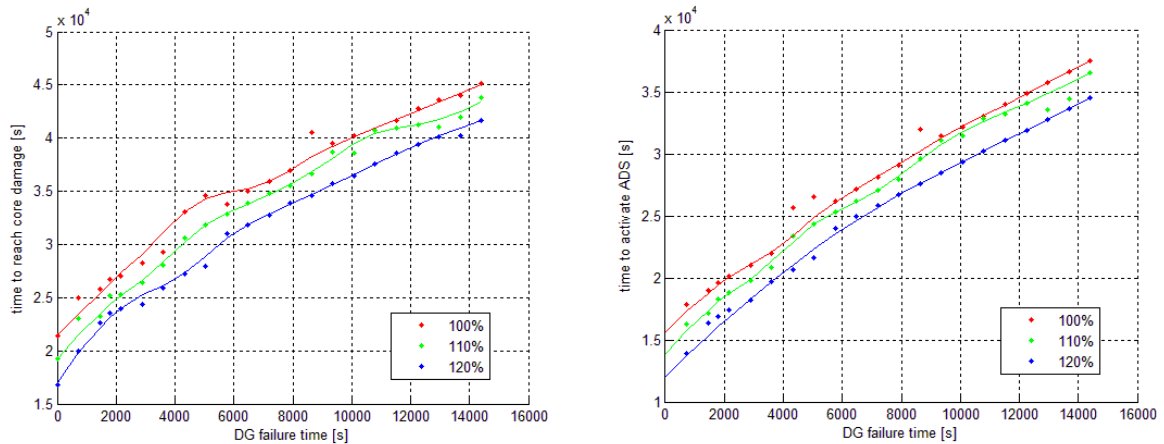


**Figure 5: Time to activate ADS vs. DG failure time (left) and time to reach core damage vs. DG failure time (right) curves for 100% 110% and 120% power**

Our second set of experiments focused on the determination on the “limit surfaces” [7,8], i.e. boundaries in the state space that separates failure from success. As a first step we focused on considering a 2-dimensional state space: FW availability time (measured after ADS activation, i.e.  $T_{FW} - T_{ADS}$ ) and battery life. By randomly changing these two parameters we observe the outcome of each simulation (failure or success) and, by using a Support Vector Machines (SVM) based classifier [7] (see Appendix A), we determine the limit surface.

Results are shown in Figure 6 for two different values of power: 100%, and 120%. As expected, a longer battery life and a shorter firewater injection alignment time lead to success, while a short battery life and long firewater alignment time failed. The slope at the left end of the success space represents situations where battery power cuts out, the SRVs de-energize and close, and the RPV re-pressurizes just before the firewater can be aligned. In order to guarantee success, a minimum battery life was needed, and a higher core power allowed for the core to remain protected with a shorter battery life where a lower power core would have failed. This is due to the fact that the simulation did not account for the possibility of a manual ADS activation, and required that the heat curves for the plant be exceeded before ADS activation. In a higher power simulation, the heat curves are exceeded more quickly, ADS is activated sooner and less battery life is needed. The trade-off to this is that the firewater must be aligned more quickly in the higher power simulations than the lower power simulations, which is not a worthwhile trade-off in a real situation, as the ADS can be activated early in a real situation if the firewater injection is ready before the heat curves are exceeded.

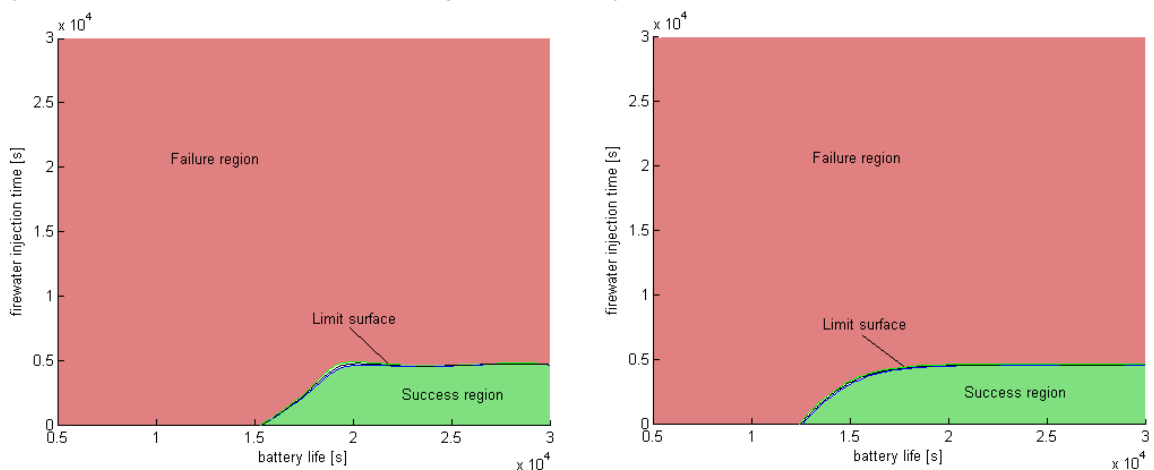


**Figure 6: FW availability time vs. Battery life: limit surface for 100% (left) and 120% (right) power**

Similarly, we determine the limit surface for a different 2-dimensional state space: DG failure time vs. AC power recovery time (either DG recovery or off-site power recovery). Thus, we sample these two parameters uniformly over the space and we observed the final outcome of the simulation (success or failure). Using the same SVM classifier we thus determined the limit surface.

For this case, we expect that core damage occurs for early DG failure time (i.e., early  $T_{SBO}$ ) and late AC recovery time. In other words we expect failure for long time interval between AC power lost and AC power recovery events.

Limit surfaces are shown in Figure 7 for three different values of power levels: 100% (left) and 120% (right). As expected, failures occur when AC power is lost for a long time and for early failure of DG.

Note that if reactor power increases, time to reach PSP HCTL limits and time to reach core damage decreases. Thus, the time that the plant operators have to recover AC power shrinks.

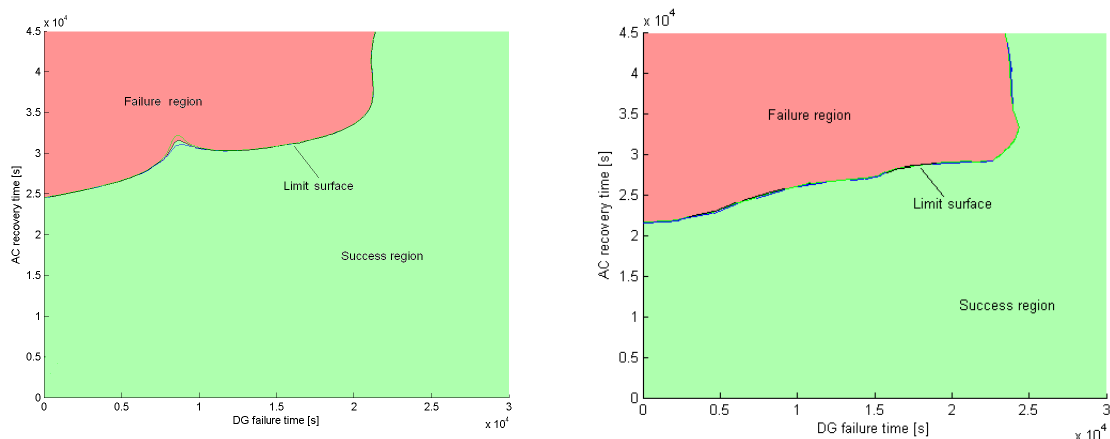


Figure 7: AC recovery time vs. DG failure time: limit surface for 100% (left) and 120% (right) power

## 5. ADAPTIVE SAMPLING

Nuclear simulations can be computationally expensive, time-consuming, and high dimensional with respect to the number of input parameters. Thus, exploring the space of all possible simulation outcomes is infeasible using finite computing resources. This limitation is a typical context for performing adaptive sampling where a few observations are obtained from the simulation, a surrogate model is built in order to predict behaviour of the system (e.g., maximum core temperature), and new samples are selected based on the model constructed (see Figure 8).

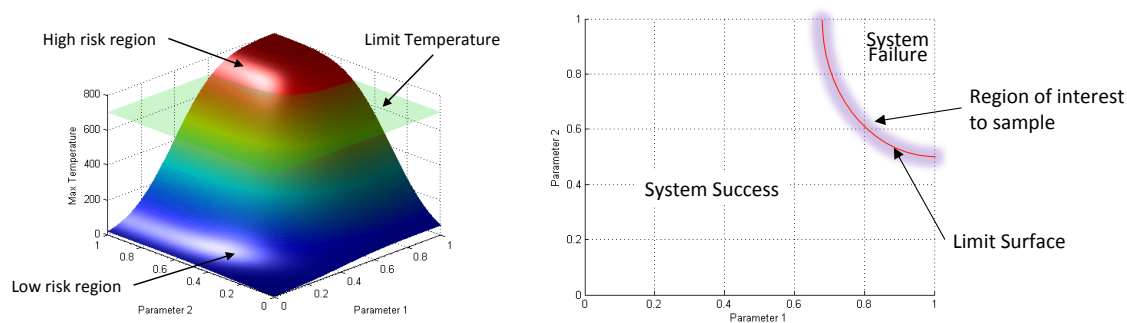


Figure 8: Max core temperature as function of 2 parameters and limit/fail temperature (left) and plot of their intersection: limit surface (right)

The surrogate model is then updated based on the simulation results of the sampled points [7,8]. In this way, we attempt to gain the most information possible with a small number of carefully selected sampled points, limiting the number of expensive trials needed to understand features of the simulation space. From a safety point of view, we are interested in identifying the limit surface, i.e., the boundaries in the simulation space between system failure and system success. The generic structure of an adaptive sampling algorithm is shown in Figure 9 (left).

For this paper, we have implemented a graph-based adaptive sampling scheme [8] (see Figure 9 right). This algorithm begins by directly building a neighbourhood structure as the surrogate model (e.g. a relaxed Gabriel graph) on the initial training data. It then creates a candidate set by first obtaining linearly interpolated points along all spanning edges of the graph, and introducing a random perturbation along all dimensions to these points.

Note that this algorithm does not employ any mathematical model (e.g., Gaussian Process Model as shown in [8]) to infer the location of the limit surface but only relies on the data point location. The graph obtained during each round changes only slightly, such that without a random perturbation, the candidate points are generally located linearly along edges of the graph, which is less desirable.

We performed a set of preliminary tests to evaluate the performance of adaptive sampling schemes. In particular, in this report, we focused on the evaluation of the limit surfaces presented in Figures 6 and 7. The results shown in Table 1 indicate a great reduction in terms of simulation runs needed in order to identify such limit surfaces.

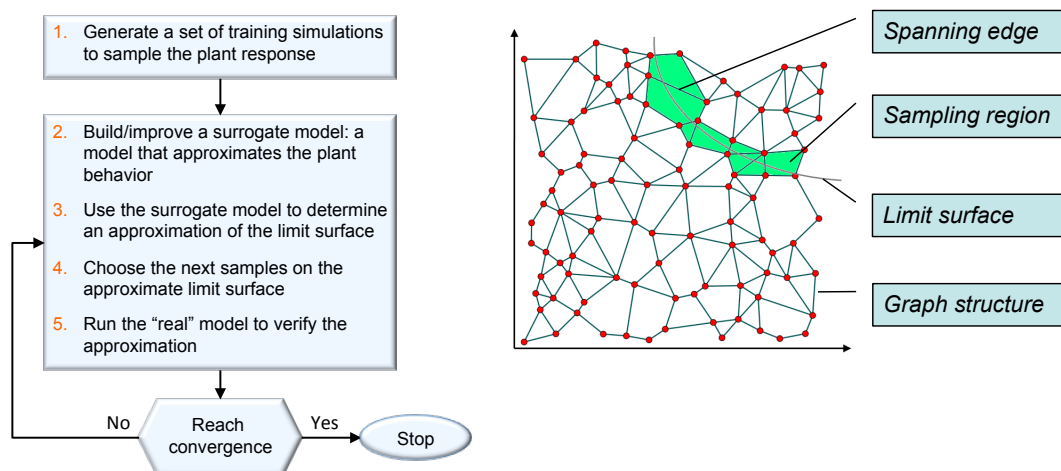


**Figure 9: Generic scheme for adaptive sampling algorithms (left) and scheme of Graph base adaptive sampling algorithm (right)**

**Table 1: Preliminary adaptive sampling results**

<i>Test case</i>	<i>Monte-Carlo sampling</i>	<i>Adaptive sampling</i>	<i>Time reduction</i>
Figure 6	700	~ 60	91.5 %
Figure 7	800	~ 60	92.5 %

## 6. STOCHASTIC ANALYSIS

The stochastic analysis for the BWR SBO test case has been performed using the code RAVEN [5,6] that is currently under development at INL. Originally, RAVEN was designed to control the code RELAP-7 but its capabilities have been extended to include also stochastic analysis methodologies (also known as dynamic PRA) such as Monte-Carlo and Dynamic Event Tree algorithms.

In addition, recently RAVEN has been coupled to RELAP-5 and RELAP-7. Such coupling allows performing multiple RELAP runs (through Monte-Carlo sampling).

The stochastic analysis (Monte-Carlo) when using RELAP-5 is performed through the following steps:

1. Probability distributions for the considered stochastic parameters are obtained from the PRA
2. A link between the considered stochastic parameters and the parameters coded in the RELAP-5 input file is established by RAVEN
3. A set of  $N$  RELAP-5 input files are generated and values for the considered stochastic parameters are randomly sampled from their own distributions and plugged in the input files
4. Through the use of high performance computing capabilities of INL, all RELAP-5 runs are distributed on all available nodes and cores
5. When all simulation runs are completed, RAVEN generates an output file (in .csv format) for each simulation for the original RELAP-5 output file
6. All .csv files generated can now be analyzed using state-of-the-art data analysis algorithms which include such as multi-dimensional data visualization tools

In order to evaluate the impact of the uncertain parameters listed in Section 3 on the simulation outcome we performed an extensive Monte-Carlo analysis that consisted of generating 20,000 Monte-Carlo runs.

## 7. UNCERTAINTIES ANALYSIS AND VISUALIZATION

We apply clustering algorithms [9,10] based on the Morse-Smale complex [11,12] on the dataset obtained from RAVEN for the BWR SBO analysis (see Appendix B). In essence, we aim to reconstruct the response surface (i.e., max clad temperature) topological structure in a  $d$ -dimensional space where  $d$  is the number of uncertain parameters.

We further obtain a topological summary for each cluster and try to infer the correlations between simulation parameters and system observations. The objective is to find the combination of conditions (in the form of input simulation parameters) that can cause core damage.

Before analysing the data we performed a series of pre-processing procedures:

- Data standardization: The above data is pre-processed with a standardization process. Since different parameters may be measured on different scales and the range of values differ from each dimension, some parameters may dominate the results of the analysis. We employ a z-score data standardization process so that all dimensions are on the same scale. For values of each dimension, we subtract the mean and divide by the standard deviation.
- Dimension reduction: Upon further observations of the nature of the simulation, we further transform the data by reducing the number of dimensions. In particular, we introduce 3 new dimensions by combining 3 pairs of dimensions from the raw dataset:
  - ACPowerRecoveryTime:  $\min \{ \text{RecoveryTimeDG}; \text{OFFsitePowerRecoveryTime} \}$ .
  - SRVstuckopen:  $\min \{ \text{SRV1stuckopen}; \text{SRV2stuckopen} \}$ .
  - CoolingFailtoRunTime:  $\max \{ \text{HPCIFailToRunTime}; \text{RCICFailToRunTime} \}$ .

The 9D case includes then the following input variables:

1. FailureTimeDG
2. ACPowerRecoveryTime
3. SRVstuckOpenTime
4. cladFailureTemperature
5. CoolingFailtoRunTime
6. Reactor power
7. ADSactivation-TimeDelay
8. firewaterTime
9. TotalBatteryLife

The output variable is the maxCladTemp (MT).

Using HDViz [11,12,14] (see Appendix C), from 9D-MT-all-3C, we were able to obtain 3 clusters as shown in Figure 10. The topological structure of the clad max temperature as a 9-dimensional surface was characterized by a single local minimum and 3 local maxima as indicated in Table 3.

Value: 1008.80  
Input std: 2.87  
Density: 0.0014  
Projection: Isomap

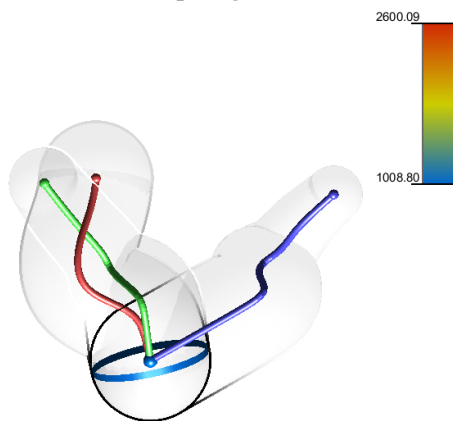


**Figure 10: Topological summary**

Figure 11 shows the projection of the three crystals for each dimension including their regression curves: x-axis corresponds to output variable (maximum clad temperature) while y-axis corresponds to input variable. From Figure 11, by looking at the regression curve obtained, we can see that a high value of clad temperature is reached, for all 3 crystals, for a late AC recovery time. As expected a late AC recovery time is a necessary condition to reach core damage. The same conclusions can be drawn for FW injection time, a late FW injection time guarantees core damage as well.

Failure time of DGs differentiates the three crystals, i.e., a late DG failure time is not sufficient to guarantee system success. In fact, by looking at the green crystal regression curve, a late failure time of DGs coupled with an early SRV stuck-open event and an early failure of the high-pressure injection system (both RCIC and HPCI) leads to core damage. By looking at the regression curve of the purple crystal, core damage condition was reached for an early DGs failure time and an early failure of the high-pressure injection system (both RCIC and HPCI).

Failure time of DGs differentiates the three crystals, i.e., a late DG failure time is not sufficient to guarantee system success. In fact, by looking at the green crystal regression curve, a late failure time of DGs coupled with an early SRV stuck-open event and an early failure of the high-pressure injection system (both RCIC and HPCI) leads to core damage. By looking at the regression curve of the purple crystal, core damage condition was reached for an early DGs failure time and an early failure of the high-pressure injection system (both RCIC and HPCI).

**Table 2: Minima and maxima of the crystals of Figure 10.**

<i>Crystal colour (see Figure 10)</i>	<i>Min</i>	<i>Max</i>
Red	1008.80	2600.09
Green	1008.80	2597.20
Blue	1008.80	2534.16

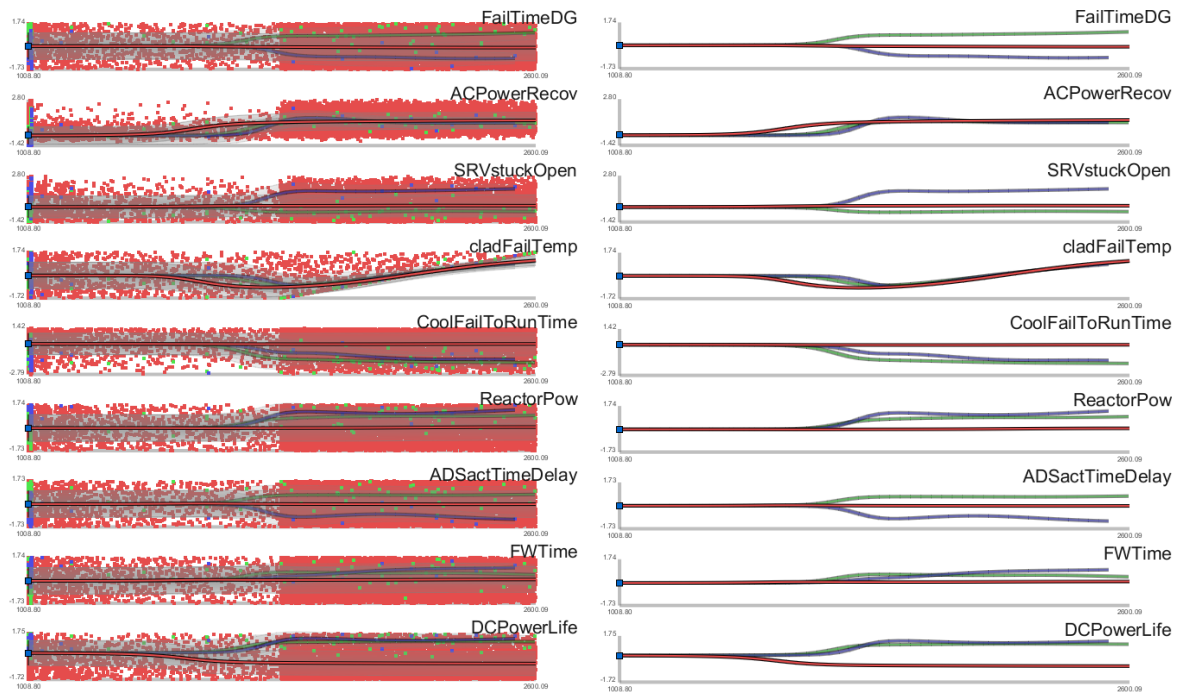


**Figure 11: Inverse coordinate plots with (left) and without (right) points projection**

## 8. CONCLUSIONS

In this paper we have summarized a series of methodologies/algorithms that are being implemented within the RISMIC project. Its main scope is to provide stakeholders with risk-informed information when power uprates and life extension of an existing plant is being considered. While some of this risk-informed information has been generated in a classical fashion, others have been produced using more advanced methodologies based upon CPRA. Lastly, we introduced the value of the limit surface associated to adaptive sampling and data analysis/visualization algorithms.

We have presented their application for a detailed BWR SBO test case in order to evaluate the impact of power uprates (to 110% and 120%) on system dynamics.

## REFERENCES

- [1] Smith, C., Rabiti, C., and Martineau, R., "Risk Informed Safety Margins Characterization (RISMIC) Pathway Technical Program Plan", INL/EXT-11-22977, Idaho National Laboratory (2012).
- [2] N. Siu, "Risk assessment for dynamic systems: an overview," *Reliability Engineering and System Safety*, **43**, no. 1, pp. 43-73 (1994).
- [3] RELAP5 Code Development Team. (2012). RELAP5-3D Code Manual. INL, (2012).
- [4] D. Mandelli, C. Smith, C. Rabiti, A. Alfonsi, J. Cogliati, and R. Kinoshita, "New methods and tools to perform safety analysis within RISMIC," in *Proceeding of American Nuclear Society (ANS)*, Washington (2013).

- [5] Alfonsi, C. Rabiti, D. Mandelli, J. Cogliati, and R. Kinoshita, "Raven as a tool for dynamic probabilistic risk assessment: Software overview," in *Proceeding of M&C2013 International Topical Meeting on Mathematics and Computation*, CD-ROM, American Nuclear Society, LaGrange Park, IL (2013).
- [6] A. Alfonsi, C. Rabiti, D. Mandelli, J. Cogliati, and R. Kinoshita, "Raven as a tool for dynamic probabilistic risk assessment," in *Proceeding of American Nuclear Society (ANS)*, Atlanta (GA), vol. 108, pp. 555-558, (2013).
- [7] D. Mandelli and C. Smith, "Adaptive sampling using support vector machines," in *Proceeding of American Nuclear Society (ANS)*, San Diego (CA), vol. 107, pp. 736-738 (2012).
- [8] D. Maljovec, B. Wang, V. Pascucci, P.-T. Bremer, and D. Mandelli, "Adaptive sampling algorithms for probabilistic risk assessment of nuclear simulations," in *ANS PSA 2013 International Topical Meeting on Probabilistic Safety Assessment and Analysis*, Columbia, SC, on CD-ROM, American Nuclear Society, LaGrange Park (IL) (2013).
- [9] D. Mandelli, A. Yilmaz, T. Aldemir, K. Metzroth, and R. Denning, "Scenario clustering and dynamic probabilistic risk assessment," *Reliability Engineering & System Safety*, **115**, pp. 146-160 (2013).
- [10] D. Mandelli, C. Smith, A. Yilmaz, and T. Aldemir, "Mining nuclear transient data through symbolic conversion," in *ANS PSA 2013 International Topical Meeting on Probabilistic Safety Assessment and Analysis*, Columbia, SC, on CD-ROM, American Nuclear Society, LaGrange Park, IL (2013).
- [11] D. Maljovec, B. Wang, V. Pascucci, P.-T. Bremer, M. Pernice, D. Mandelli, and R. Nourgaliev, "Exploration of high-dimensional scalar function for nuclear reactor safety analysis and visualization," in *Proceeding of M&C2013 International Topical Meeting on Mathematics and Computation*, CD-ROM, American Nuclear Society, LaGrange Park, IL (2013).
- [12] D. Maljovec, B. Wang, D. Mandelli, P.-T. Bremer and V. Pascucci, "Analyzing Dynamic Probabilistic Risk Assessment Data through Topology-Based Clustering," in *ANS PSA 2013 International Topical Meeting on Probabilistic Safety Assessment and Analysis*, Columbia, SC, on CD-ROM, American Nuclear Society, LaGrange Park (IL) (2013).
- [13] D. Gertman, H. Blackman, J. Marble, J. Byers, and C. Smith, "The SPAR-H Human Reliability Analysis Method", NRC (2005).
- [14] S. Gerber, P.-T. Bremer, V. Pascucci, and R. T. Whitaker, "Visual exploration of high dimensional scalar functions", *IEEE Transactions on Visualization and Computer Graphics*, vol. 16, pp. 1271-1280 (2010).

## APPENDIX A: LIMIT SURFACE DETERMINATION

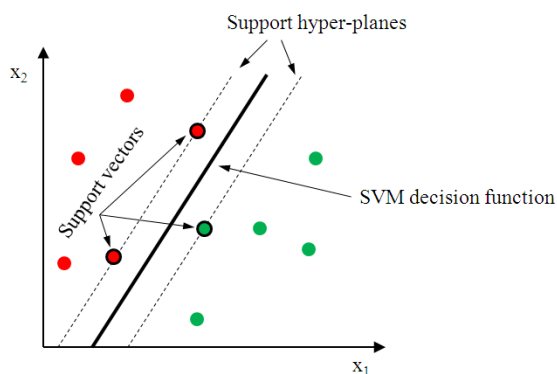


Figure 12: Limit surface evaluation using SVMs

Given a set of  $N$  multi-dimensional samples  $\mathbf{x}_i$  and their associated results  $y_i = \pm 1$  (e.g.,  $y_i = +1$  for system success and  $y_i = -1$  for system failure), the SVM finds the boundary (i.e., the decision function) that separates the set of points having different  $y_i$ . The decision function lies between the support hyper-planes that are required to: pass through at least one sample of each class (called support vectors) and not contain samples within them. For the linear case, see Figure 12, the decision function is chosen such that distance between the support hyper-planes is maximized.

Without going into the mathematical details, the determination of the hyper-planes is performed recursively and updated every time a new sample has been generated. Figure 12 shows the SVM decision function and the hyper-planes for a set of points in a

2-dimensional space having two different outcomes:  $y_i = +1$  (green) and  $y_i = -1$  (red). The transition from a linear to a generic non-linear hyper-plane is performed using the kernel trick. This process involves the projection of the original samples into a higher dimensional space known as feature space generated by kernel functions  $K(\mathbf{x}_i, \mathbf{x}_j)$ .

## APPENDIX B: MULTI-DIMENSIONAL DATA VISUALIZATION

The need for software tools able to both analyze and visualize large amount of data generated by Dynamic PRA methodologies has been emerging only in recent years. In the past 2 years, INL and the University of Utah have developed a software tool able to analyze multi-dimensional data: HDViz. HDViz models the relations between output variables (e.g., maximum clad temperature) and stochastic/uncertain parameters as high-dimensional functions. In this respect, HDViz segments the domain of these high-dimension functions into regions of uniform gradient flow by decomposing the data based on its approximate Morse-Smale complex (see Figure 13). Points (i.e., simulation runs) belonging to a particular segmentation have similar geometric and topological properties, and from these it is possible to create compact statistical summaries of each segmentation. Such summaries are then presented to the user in an intuitive manner that highlight features of the dataset that are otherwise hidden.

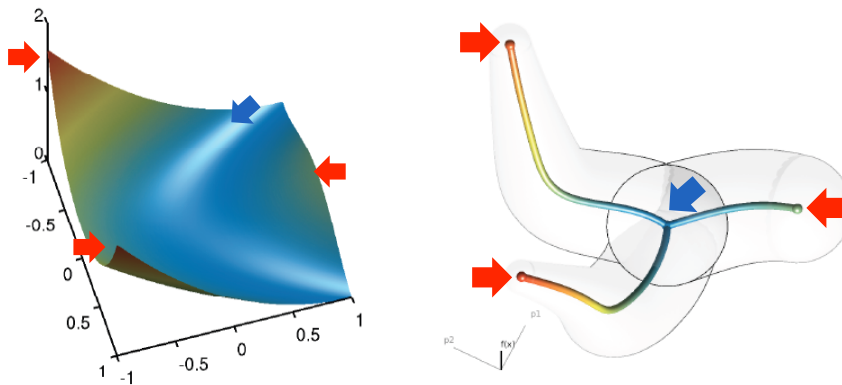


**Figure 13: Representation example of a 2-dimensional function in terms of crystals that connect local minima to local maxima. In this case, a single minima (blue arrow) and 3 maxima (red arrows) have been identified. Three crystal have also been determined; each one showing the path that connect a local minima to a local maxima**